Biomaterials 29 (2008) 3429–3437

Contents lists available at ScienceDirect

Biomaterials

journal homepage: www.elsevier.com/locate/biomaterials

Observations on the microvasculature of bone defects filled with biodegradable nanoparticulate hydroxyapatite

Olaf Kilian [a,*], Sabine Wenisch [c], Srikanth Karnati [d], Eveline Baumgart-Vogt [d], Anne Hild [c], Rosemarie Fuhrmann [b], Tarja Jonuleit [e], Elvira Dingeldein [f], Reinhard Schnettler [a], Ralf-Peter Franke [b,g]

[a] Department of Trauma Surgery, University of Giessen, Rudolf-Buchheim-Strasse 7, 35392 Giessen, Germany
[b] Department for Biomaterials, University of Ulm, Germany
[c] Laboratory of Experimental Trauma Surgery, University of Giessen, Germany
[d] Institute for Anatomy and Cell Biology II, Division of Medical Cell Biology, University of Giessen, Germany
[e] CellMed AG, Alzenau, Germany
[f] Osartis GmbH, Obernburg, Germany
[g] Berlin-Brandenburg Center for Regenerative Therapies, Charité Campus Virchow, University of Berlin, Germany

ARTICLE INFO

Article history:
Received 28 February 2008
Accepted 6 May 2008
Available online 23 May 2008

Keywords:
Angiogenesis
Endothelial cell
Lymphatic vessel
Hydroxyapatite composite
Platelet
Animal model

ABSTRACT

The microvascularization of metaphyseal bone defects filled with nanoparticulate, biodegradable hydroxyapatite biomaterial with and without platelet factors enrichment was investigated in a minipig model. Results from morphological analysis and PECAM-1 immunohistochemistry showed the formation of new blood vessels into the bone defects by sprouting and intussusception of pre-existing ones. However, no significant differences were observed in the microvascularization of the different biomaterials applied (pure versus platelet factors-enriched hydroxyapatite), concerning the number of vessels and their morphological structure at day 20 after operation. The appearance of VEGFR-2 positive endothelial progenitor cells in the connective tissue between hydroxyapatite particles was also found to be independent from platelet factors enrichment of the hydroxyapatite bone substitute. In both groups formation of lymphatic vessels was detected with a podoplanin antibody. No differences were noted between HA/PLF− and HA/PLF+ implants with respect to the podoplanin expression level, the staining pattern or number of lymphatic vessels. In conclusion, the present study demonstrates different mechanisms of blood and lymphatic vessel formation in hydroxyapatite implants in minipigs.

1. Introduction

The integration of bone graft material during ossification of bone defects depends on the implants' microvascularization [1–3]. Investigations of the embryogenesis, oncogenesis and wound healing have shown various possible angiogenetic mechanisms that result in neoformation of vessels [4–7].

Angiogenesis is defined as the process of capillary formation by intussusception or invagination in pre-existing vessels [8–10]. Intussusception is commenced by the proteolysis of the vessels intima which results in vasodilatation and fenestration of the vessels' basal lamina. The induced increase in permeability leads to extravascularisation of plasma proteins like fibrinogen and plasminogen, both necessary as matrix for endothelial cell migration [11]. Lumina of vessels are formed by proliferation and adhesion of endothelial cells. The maturation of newly formed vessels is characterized by the completion of the basal lamina. Their stabilization is induced by extracellular matrix proteins, e.g. fibronectin [12], and the adhesion of α-smooth muscle actin-positive pericytes [13]. During the process of intussusception, invagination of opposing capillary walls extends into the lumen and thereby building a bilayer. The perforated bilayer allows endothelial cells, fibroblasts or pericytes to penetrate into the lumen which provides an extracellular matrix and finally split the single vessel into two [9,10,14]. To date, intussusceptive newly vessel formations have been observed only in the pulmonary circulation [15] and skeletal muscles [16].

Vasculogenesis can be defined as the process of differentiation of endothelial cells derived from haemotopoietic precursor cells called angioblasts, which are positive for VEGFR-2 (Flk-1) [17–20]. Angioblasts migrate and merge close to the blood clots and finally differentiate into endothelial cells to develop a primitive vessel tube. There is a final maturation of the vascular tree by pruning and extension through angiogenesis, and by completion of the basal lamina and adhesion of pericytes.

During embryogenesis both mechanisms of vessel neoformation exist. The postnatal formation of new vessels is also achieved by

* Corresponding author. Tel.: +49 641 9944601; fax: +49 641 9944609.
E-mail address: olaf.kilian@chiru.med.uni-giessen.de (O. Kilian).

0142-9612/$ – see front matter © 2008 Elsevier Ltd. All rights reserved.
doi:10.1016/j.biomaterials.2008.05.003

vasculogenesis in endodermal tissue of the lung [21], while angiogenesis dominates in ectodermal and mesodermal development of the kidneys [6]. Previous reports suggest that endothelial cells are capable of forming a system of veno-lymphatic vessels [22–24]. However, knowledge on the molecular mechanisms during lymphangiogenesis is not available to date. Edwards et al. [25] could only detect lymphatic vessels in connective tissue overlying the periosteum, but not in cortical or cancellous bone.

To our knowledge, the role of biomaterial-associated lymphatic vessel formation has not been well investigated. Formation of new vessels is regulated by cell adhesion molecules, e.g. PECAM-1, and cytokines, e.g. VEGF, bFGF, and PDGF [9,17,26–29]. By application of an excess of growth factors, the process can also be overstimulated leading to uncontrolled vessel formation [9]. Earlier investigations of the microvascularization during fracture healing in diaphyseal bone have demonstrated blood vessel formation by sprouting and vasculogenetic processes [20].

Thus, our study aims were to investigate the molecular mechanisms and morphology of the microvasculature, including lymphangiogenesis of metaphyseal bone defects filled with biodegradable nanoparticles of hydroxyapatite implants in miniature pigs. Further, additional effects of autologous platelet factors on microvascularization of implants were tested.

2. Materials and methods

2.1. Nanoparticulate biodegradable hydroxyapatite

The hydroxyapatite (HA) used in the present study is the fully synthetic nanoparticulate paste Ostim® (Coripharm, Obernburg, Germany) and consists of a suspension of pure hydroxyapatite in water prepared by a wet chemical reaction. The needle shaped hydroxyapatite crystals with a size of 21 nm in a-direction and of 36 nm in c-direction form agglomerates. Phase purity of the hydroxyapatite was determined by X-ray-diffraction which showed conformity with pure HA and an average crystallite size of 18 nm. The atomic ratio of calcium:phosphorus is 1.67. Ostim® paste does not harden after application into the bone and is free of endothermal heating in contrast to calcium phosphate bone cements [30,31].

2.2. Animal models

The study protocol was approved by an independent institutional review board prior to surgery. A total of 28, 9-month-old male Lewe miniature pigs (SBMF Laboratories, Dresden, Germany) were used for the current randomized study in which a cylindrical defect with a diameter of 8.9 mm and a depth of 10 mm was created in the subchondral region of the right femur condyle using a saline cooled diamond bone-cutting system (DBCS, Stryker, Duisburg, Germany). Miniature pigs were divided into two groups. The defects in pigs of group 1 were filled with pure hydroxyapatite (HA/PLF−). The animals of group 2 received composites of hydroxyapatite, enriched with platelet factors (HA/PLF+) in a 10:1 ratio of HA to PLF (1.8 ml Ostim® 33% + 0.3 ml platelet factors). After 10 or 20 days under general anaesthesia, operated animals were euthanasized by intravenous application of embutramid mebezonium iodide tetracaine (T 61®, CliniPharm, Zürich, Switzerland). For morphological investigations three animals per group were perfused through the femoral artery with 600 ml of heparinized Ringer solution, followed by 600 ml 4% paraformaldehyde (PFA) in 1% phosphate buffered saline (PBS). After euthanasia distal femora of all animals containing the defect areas was removed, dissected and stripped free of all soft tissues. The implant with neighbouring original bone of each femur was transversally cut into four specimens which were subjected to different fixation methods for further investigation. For light microscopical, immunohistochemistry and immunofluorescence preparations, all samples were additionally fixed in 4% PFA overnight. Thereafter, the samples were carefully washed with phosphate buffered saline (PBS), decalcified for 6 weeks in EDTA and embedded in paraffin. For electron microscopic investigations the samples were additionally fixed overnight in Yellow-Fix (4% paraformaldehyde, 2% glutaraldehyde, 0.04% picric acid) and embedded in Epon. Snap-frozen unfixed samples were used for PCR and Western blots.

2.3. Autologous platelet factor (PLF)

One hundred and fifty ml of peripheral blood of the external jugular vein was centrifuged at 100*g* for 10 min at RT. Platelet-rich plasma was separated and again centrifuged at 300*g* for 10 min, followed by withdrawal of the plasma and another centrifugation step at 1000*g* for 30 min. The platelet-rich plasma supernatant was carefully transferred into a preconnected bag for further preparation of the growth factors. One thousand IU thrombin (Gentrac Inc., Middleton, Massachusetts, USA) and 10 ml of 8.4% calcium-gluconate (Braun Melsungen AG, Melsungen, Germany) were added for aggregation and degranulation of the platelets. After degranulation, the liquid supernatant was filled into tubes and stored at −20 °C. The plasma was heat-inactivated at 65 °C for 30 min and again centrifuged at 1000*g* for 30 min at RT. The liquid supernatant was then transferred into tubes and stored at −20 °C.

For measurements of platelet cytokines PDGFs (AA, BB, AB), TGF-β_1, VEGF, IGFs (I, II), EGF and bFGF, Quantikine™ ELISA-kits (R&D Systems Minneapolis, Minnesota, USA) were used (Table 1).

2.4. Isolation of RNA

Total RNA isolation from snap-frozen granulation tissue of implants (HA/PLF− and HA/PLF+) was performed according to the manufacturers' guidelines with Trizol isolation reagent (Invitrogen, Karlsruhe, Germany). The yield of total RNA was determined in a BioPhotometer (Eppendorf, Hamburg, Germany) using UV measurement. DNase digestion was done by incubation with RNasefree DNase at 37 °C for 30 min. The yield of total RNA was finally determined spectroscopically at a wavelength of 280 nm.

2.5. Reverse transcription

Reverse transcription was carried out in a T3 Thermocycler (Biometra, Göttingen, Germany) using the method described by Welter et al. [32], the reaction condition was as follows: 2 μg of total RNA, 2.5 μM random hexamers (Invitrogen, Karlsruhe, Germany), 25 μM of each dNTP (Roche, Mannheim, Germany), 1 × RT buffer and M-MLV reverse transcriptase (Promega, Madison, Wisconsin, USA), incubation at 37 °C for 10 min and 75 °C for 5 min. The reverse transcription reaction was stopped by heating to 92 °C for 2 min.

2.6. PCR reaction

Commercially synthezised primers (MWG, Ebersberg, Munich, Germany) used to amplify specific porcine mRNA-transcripts [32] are described in Table 2.

The annealing temperature of each primer pair was optimized in a T3 Thermocycler (Biometra, Göttingen, Germany). A volume of 2 μl of each transcribed cDNA-preparation and 5 U of AmpliTaq Gold 1000 kit (Biosystems, Middletown, Massachusetts, USA) were used for PCR reaction. Amplicons were generated with an initial denaturation step (99 °C, 2 min) and 35 cycles of denaturation at 94 °C for 45 s, annealing at 60 °C for 45 s, extension at 72 °C for 45 s, followed by a final extension step of 2 min at 72 °C. The PCR products were analyzed by gel electrophoresis in a 2% agarose gel with 1 μg/ml ethidium bromide. Water was used instead of cDNA as a negative control.

2.7. Western blot

The specificity of the anti-VEGFR-2 (Flk-1) antibody was tested by Western blotting. Total proteins of homogenates were extracted from snap-frozen specimens of the distal minipig femora with Trizol (Invitrogen, Karlsruhe, Germany) and dissolved in Laemmli sample buffer (Sigma–Aldrich, Munich, Germany). Proteins were separated by means of SDS-PAGE by using a 10% acrylamide gel (Invitrogen, Karlsruhe, Germany). As marker, the dual color standard marker (BioRad Lab., Hercules, California, USA) with specific weight of 250 kDa was applied. The separated proteins were transferred by electroblotting with a Hybond PVDF membranes (Amersham Biosciences, Piscataway, New Jersey, USA). Non-specific protein binding sites were blocked with PBS containing 5% BSA buffer (Merck, Darmstadt, Germany) and were incubated with mouse anti-VEGFR-2 (Flk-1) antibody (Santa Cruz, Heidelberg, Germany, diluted 1:100) overnight at 4 °C. After several washes in PBS, containing 1% BSA and 1% Tween 20 (Sigma, Taufkirchen, Germany), the membranes were incubated with the secondary antibody (mouse anti-rabbit IgG, DAKO, Hamburg, Germany, diluted 1:500) for 45 min, before careful washing in TRIS-buffer. For visualization of the antigen–antibody complexes the APAAP method was used.

Table 1
Concentration of platelets (pt/ml) and various growth factors (pg/ml) in the applied mixture of platelet factors

Platelets	1,021,900 ± 345,956
TGF-β_1	69,000 ± 20,500
PDGF-AA	639 ± 423
PDGF-BB	578 ± 486
PDGF-AB	162,000 ± 68,500
VEGF	<10
bFGF	110 ± 85
EGF	311 ± 220
IGF-I	57,000
IGF-II	284

Table 2
Primers used for RT-PCR

	Primer	Product length
VEGF		
Forward	5′-ACGAAGTGGTGAAGTTCATGG-3′	$VEGF^{164}$ 318 bp
Reverse	5′-TTTTTGCAGGAACATTTACACG-3′	$VEGF^{188}$ 389 bp
		$VEGF^{205}$ 441 bp
VEGFR-2 (Flk-1)		
Forward	5′-AGACTGGTTCTGGCCCAAC-3′	379 bp
Reverse	5′-GAAGCCTTTCTGGCTGCTC-3′	

2.8. Histology

Undecalcified samples were embedded in methylmethacrylate and 20 μm sections were cut with an osteotome Exakt 340P (Exakt, Norderstedt, Germany) as described by Donath and Breuner [33]. Subsequently, the sections were stained with toluidine blue (Chroma Therapeutics Ltd, Abingdon, UK) for 10 min at RT.

2.9. Immunohistochemical staining

Demineralized samples were embedded into paraffin and 5 μm sections were cut with a rotation microtome Leica RM 2145 (Leica Instruments, Nussloch, Germany). The samples were incubated overnight either with (a) rabbit anti-human VEGF antibody (Acris, Diagnostic Products Co. Biermann, Bad Nauheim, Germany, diluted 1:50), (b) rabbit anti-human VEGFR-2 (Flk-1) antibody (Assay Designs, Ann Arbor, Michigan, USA, diluted 1:50), or (c) goat anti-mouse PECAM-1 antibody (Santa Cruz Biotechnology, Santa Cruz, California, USA, diluted 1:600) at 4 °C. The secondary biotinylated anti-rabbit and anti-goat antibodies (Dako, Glostrup, Denmark, dilution 1:50) in 3% FCS and 12% pig serum were applied for 30 min at RT. Rinsing with PBS was followed by labelling with the ABC complex/horseradish peroxidase labelled avidin (Dako, Glostrup, Denmark) for another 30 min. The chromogen Nova Red (Vector Laboratories, Burlingame, California, USA) was used for visualization of the peroxidase activity. Counterstaining of nuclei was done with hematoxylin (Shandon Scientific Ltd, Cheshire, UK).

2.10. Transmission electron microscopy

For ultrastructural examinations, small samples of the removed implants were postfixed at 4 °C for 24 h in Yellow-Fix (4% paraformaldehyde, 2% glutaraldehyde, 0.04% picric acid). After rinsing (3 × 5 min) in 0.1 M phosphate buffer (pH 7.2) the specimens were postfixed in 1% osmium tetroxide (OsO_4) for 2 h at RT, washed carefully several times in 0.1 M phosphate buffer (pH 7.2), and subsequently dehydrated in a series of graded ethanol. Thereafter, the samples were embedded in Epon 812 (Serva, Heidelberg, Germany). Polymerization was done at 60 °C for 48 h. Semithin sections (1 μm) were cut with an Ultracut R Ultramicrotom (Leica, Bensheim, Germany) and stained with Richardson's stain (1% methylene blue, 1% borax, 1% azure II). Specific regions of interest in the blocks were trimmed before cutting ultrathin sections (80 nm) with a diamond knife (45°, Diatome, Switzerland). Ultrathin sections were contrasted for 10 min with uranyl acetate and lead citrate in a Reichert Ultrastainer (Leica, Bensheim, Germany) and examined in a Zeiss EM 109 (Zeiss, Oberkochen, Germany) transmission electron microscope.

2.11. Immunofluorescence and confocal laser scanning microscopy

Five μm paraffin sections were deparaffinized with xylene (Merck, Darmstadt, Germany) (3 × 5 min), followed by rehydration in a series of ethanol. For antigen retrieval and improved accessibility of epitopes rehydrated sections were subjected to 0.01% trypsin (Sigma, Steinheim, Germany) digestion for 10 min at 37 °C, followed by irradiation for 3 × 5 min in citrate buffer (pH 6) in a microwave oven (850 W) and subsequent cooling for 60 min at RT. After blocking of non-specific protein binding sites with 4% bovine serum albumin in phosphate buffered saline with 0.05% Tween 20 (PBST), sections were incubated overnight with a monoclonal hamster antiserum against podoplanin (Acris, Hiddenhausen, Germany, diluted 1:250), a marker for lymphatic endothelial cells [34]. Antigen–antibody complexes were revealed with Alexa647-labeled anti-hamster IgG (Molecular Probes, Eugene, USA, diluted 1:500). All intermediate washing steps (3 × 5 min) and antibody dilutions were done in PBST. For negative controls, parallel sections were incubated without primary antibody followed by identical secondary antibody and washing steps. All sections were mounted in Mowiol 4-88 (Hoechst, Frankfurt, Germany) with 0.5% *N*-propylgallate. All sections were analyzed using a Leica TCS SP2 confocal microscope (Leica Microsystems, Heidelberg, Germany) using the 633 nm laser line for excitation and a window of 650–665 nm for emission collection. Images were taken with a 63× objective, setting of Airy 1 (=pinhole of 190 μm) and 64 times sampling. Tif-images were processed with Adobe Photoshop (version 6) on a Microsoft windows computer.

2.12. Statistical analysis

For statistical analysis six animals per group, three slides per animal and nine regions of interest per slide were randomly selected. The number of PECAM-1 labelled sprouting and intussusceptive vessels in HA/PLF− and HA/PLF+ implants were counted by using a scanning ocular with a field of 1.625 mm^2 and a 20× objective. Data were analyzed by independent *t*-test. Confidence levels of >95% ($p < 0.05$) were considered to be significant.

3. Results

In the interface area between host bone and implant and also between HA-particles the majority of vessels revealed a diameter of about 20 μm. However, also frequently sinusoid-like vessels with a diameter of above 100 μm were observed. Newly developed vessels next to the biomaterial were found in close vicinity to hydroxyapatite nanoparticles and the newly formed woven bone (Fig. 1A). Dilated vessels showed sprouting extensions and invagination of opposing capillary walls (Fig. 1B and C).

Immature newly developed vessels next to the biomaterial nanoparticles could be identified due to their incomplete basal lamina, a thin endothelium and the absence of pericytes (Fig. 2A).

In contrast, the wall of mature capillaries was formed by a single endothelium surrounded by a complete basal lamina. In endothelial cells of mature capillaries typical endocytotic/transcytotic vesicles and fenestrations were found, possibly involved in nutrient- and ion-exchange between vascular and perivascular tissues. The endothelial fenestrations were plasma membrane microdomains which appeared as circular discontinuities of about 60 nm in diameter. In addition, desmosomes were observed between two adjacent endothelial cells, which are characterized by the dense cytoplasmic plaques and are interconnected with the intermediate filament system (Fig. 2B and C).

Intussusceptive vessel formation next to the biomaterial was demonstrated with PECAM-1 staining (Fig. 3A) and transmission electron microscopy (Fig. 3B–D), suggestive for invaginations of opposing endothelium and sprouting of the cells into the bilayer.

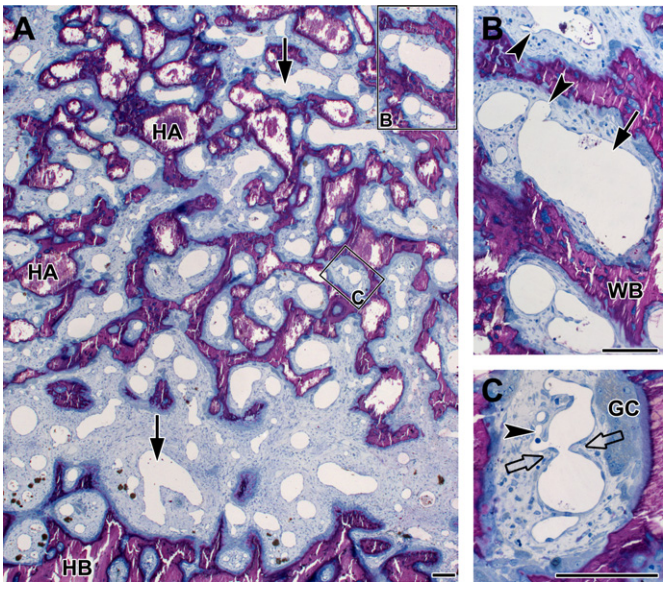

Fig. 1. Microvascularization of nanoparticulate hydroxyapatite implants. HA/PLF+, day 20 after implantation, and (A) sinusoid-like vessels with irregular diameter up to 100 μm (black arrow) in the interface area between host bone and implants and between hydroxyapatite particles in comparison to vessels with normal diameter of about 20 μm. (B) Sprouting extensions (black arrowheads) of dilated vessels (black, thin arrow). (C) Invagination of capillary walls (transparent arrows) and sprouting (black arrowheads). Semithin section, all bars = 50 μm, EC = endothelial cell, GC = giant cell, HA = hydroxyapatite particle, WB = woven bone, and HB = host bone.

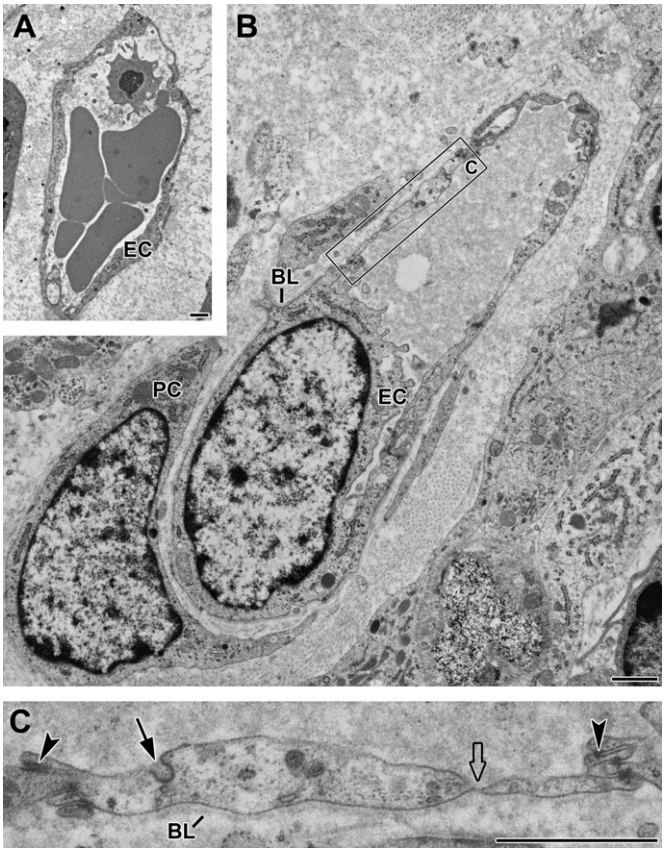

Fig. 2. (A) Newly formed, immature vessel in endothelial cell containing hydroxyapatite bone substitute material, with thin endothelium, no basal lamina, HA/PLF−, and day 20 after implantation. (B) Mature vessel with complete basal lamina and adhesion of a pericyte. (C) Fenestrated endothelium (transparent arrow), membrane-vesiculation (black, thin arrow), and adherent junctions with desmoplakin (black arrowheads) of two endothelial cells, transmission electron microscopy, all bars = 1 μm, HA/PLF+, and day 10 after implantation. EC = endothelial cell, BL = basal lamina, and PC = pericyte.

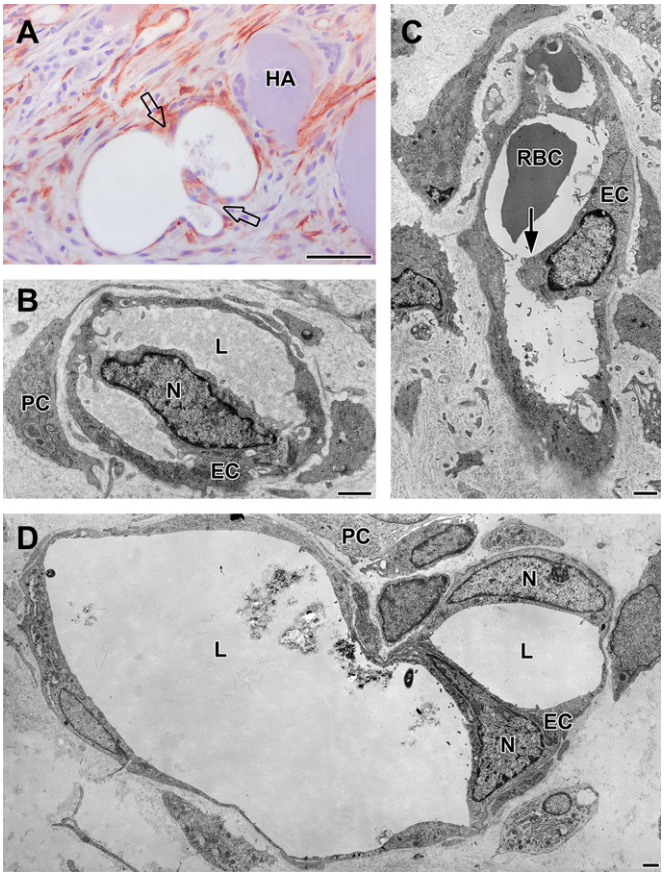

Fig. 3. (A) Invagination of opposing capillary walls (transparent arrows) near hydroxyapatite particles. PECAM-1 immunostaining, bar = 50 μm, HA/PLF−, and day 20 after implantation. (B) Complete and (C) incomplete intussusception (black arrow) with protrusions of opposing vessel capillary walls into the vessel lumen, endothelial bilayer becomes perforated and transluminal pillars are formed. (D) Two mature vessels after the intussusceptive process with intravasal debris. Transmission electron microscopy, all bars = 1 μm, HA/PLF−, and day 20 after implantation. HA = hydroxyapatite particle, EC = endothelial cells, N = nucleus, L = lumen, PC = pericyte, and RBC = red blood cell.

VEGF^{189}-, VEGF^{205}- and VEGFR-2 (Flk-1)-mRNA were identified by RT-PCR in porcine granulation tissue of HA/PLF− and HA/PLF+ implants. VEGF^{189}-mRNA was detected with a corresponding amplicon size of 389 bp and VEGF^{205}-mRNA of 441 bp. The presence of the mRNA encoding VEGFR-2 (Flk-1) was detected by amplicon size of 379 bp (Fig. 4A). Western blot analysis with a mouse-anti-VEGFR-2 antibody revealed immunoreactive bands corresponding to the VEGFR-2 (Flk-1) protein in porcine granulation tissue at correct molecular weight (Fig. 4B).

In both implant groups immunohistochemical investigations of hydroxyapatite particles-associated granulation tissue for the VEGFR-2 protein showed positive labelling of endothelial cells and of putative endothelial progenitor cells (angioblasts) (Fig. 4C). Between both groups no significant differences were observed.

Progenitor cells revealed round, enchromatic nuclei in comparison to mature endothelial cells endothelial with elongated, more heterochromatic nuclei. At day 10 after implantation sprouting extensions of merged angioblasts still existed exhibiting a discontinuous endothelium surrounding erythrocytes (Fig. 5A). Maturation of preformed vessel tubes was continued by the development of the complete basal lamina and adhesion of pericytes. These pericytes exhibited protrusions-like contacts to the adjacent basal lamina (Fig. 5B and C).

Venous valves (Valvulae venosa) with their characteristic pair wise disposed halfmoon-shaped intima foldings could not be demonstrated, neither in venules nor in lymphatic vessels. PECAM-1 staining of newly formed vessels in HA/PLF− and HA/PLF+ implant groups showed no significant differences of sprouting or intussusceptive processes (Fig. 6).

Lymphatic vessels were identified by their typical morphology in toluidine blue stained semithin sections (Fig. 7A and B) or by transmission electron microscopy (Fig. 7C–E). These lymphatic vessels were about 30 μm in diameter and characterized by discontinuous endothelial layers, either with open into the neighbouring connective tissue (Fig. 7A and E) or showing blind-ended sprouting (Fig. 7B). In comparison to mature blood capillaries, lymphatic vessels did nether possess a continuous basal lamina nor attract α-smooth muscle actin-positive pericytes. Frequently, macrophages showing signs of degeneration were detected in the vicinity of the lymphatic vessels (Fig. 7C and D).

In addition, the newly formed lymphatic vessels exhibited positive labelling for podoplanin, a specific marker for the lymphatic endothelium (Fig. 8). No significant differences were noted between HA/PLF− and HA/PLF+ implants with respect to the podoplanin expression level, the staining pattern or number of lymphatic vessels (Fig. 8A and B). Labelling for podoplanin was very specific since endothelial cells of blood capillaries, as well as the adjacent connective tissue, the hydroxyapatite particles and the surrounding matrix were completely negative. Afferent lymphatic vessels of a porcine lymph node were used as positive control

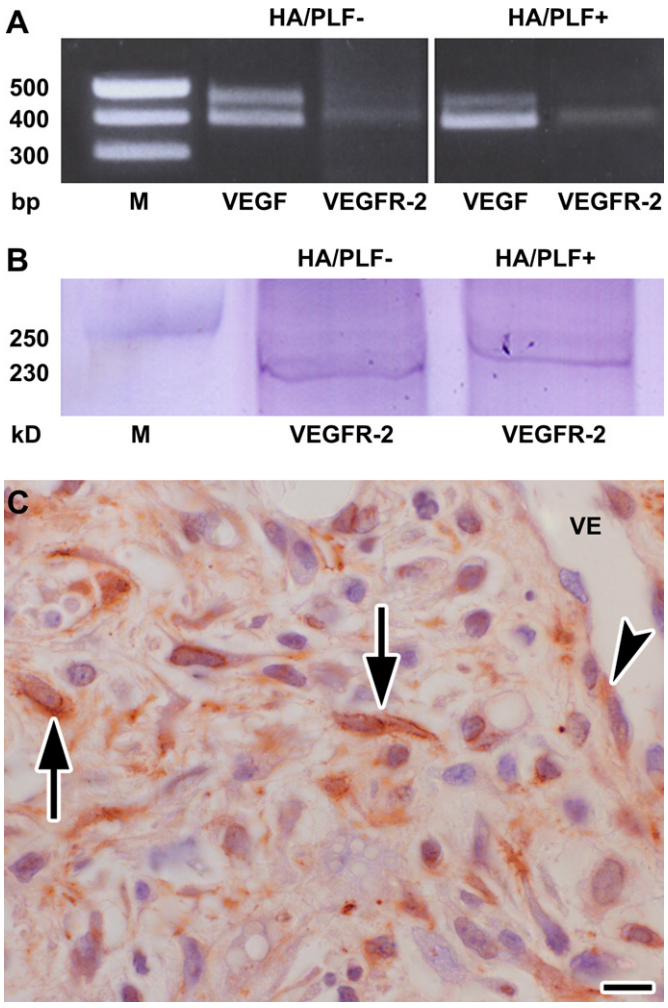

Fig. 4. (A) Specific RT-PCR products for $VEGF^{205}$ (441 bp), $VEGF^{189}$ (389 bp), and VEGFR-2 (Flk-1) (379 bp), and (B) Western blot analysis of VEGFR-2 (Flk-1) (200–230 kDa) in porcine granulation tissue of HA/PLF− and HA/PLF+ implants. The results are representative example on three independent experiments. (C) VEGFR-2 (Flk-1) positive cells in endothelium (black arrowhead), in granulation tissue (black arrows) between hydroxyapatite particles, VEGFR-2 (Flk-1) immunostaining, bar = 10 μm, HA/PLF+, day 20 after implantation, and VE = vessel.

(Fig. 8C). All negative controls were devoid of reaction products (data not shown).

4. Discussion

In our study, we investigated morphological mechanisms of microvascularization in biodegradable nanoparticulate hydroxyapatite implants, which were used in a metaphyseal bone defect in a porcine animal model. By using intravital fluorescence microscopy, Laschke et al. [35] described an increased new vessel formation in a hamster model between days 6 and 14 after implantation of the nanoparticulate bone substitute material Ostim®, which was also used in our study. They suggested that degraded areas of Ostim® permitted the direct invasion of newly formed vessels into the biomaterial, which might be specifically promoted by the high water content of the applied biomaterial. We speculated that this phenomenon could be explained in addition by a release of angiogenetic cytokines in the post-inflammatory phase of the defect healing. Therefore, we used the Ostim® biomaterial, substituted with and without platelet factors and appropriate timepoints (days 10 and 20 after implantation of the biomaterial) for the investigation of early vessel formation in a minipig model.

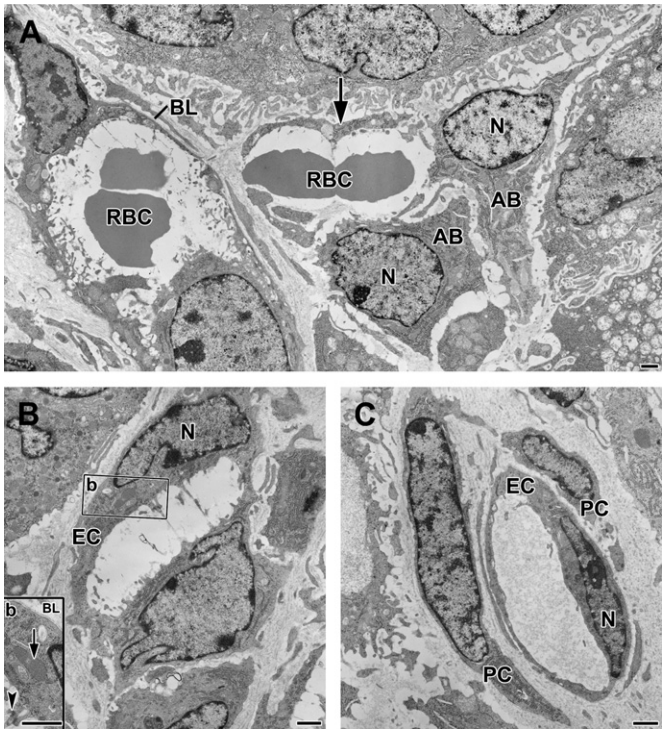

Fig. 5. (A) Merging of angioblasts and formation of a lumen by endothelial extensions, immature vessel with incomplete basal lamina (black arrow), (B) vessel tube with (b) complete basal lamina (black arrow) and Weibel–Palade body (black arrowhead). (C) Mature vessel with complete basal lamina, adherent pericyte and elongated endothelial cell nucleus. Transmission electron microscopy, all bars = 1 μm, HA/PLF−, day 10 after implantation, AB = angioblast, RBC = red blood cell, N = nucleus, BL = basal lamina, EC = endothelial cell, and PC = pericyte.

To our knowledge, we could demonstrate for the first time sprouting and non-sprouting angiogenic processes in synthetic, nanoparticulate hydroxyapatite bone substitute materials. As early as on day 10 post-operatively, sinusoid-like vessels with upto four times increased diameters compared to normal vessels of bone were identified in the interface area between normal bone stock, biomaterial and hydroxyapatite particles. The dilated vessels partly contained fenestrated basal laminae as described earlier by Bussolino et al. [8] as a result of proteolytic endothelial degradation. Plasma proteins can penetrate through these fenestrae into the perivascular space and initiate a matrix for endothelial cell migration and targeting of cytokines and growth factors for regulating cell function and angiogenesis. Adhering endothelial cells can develop adherence junctions followed by the characteristic placement of anchor proteins in the cell membrane detectable as dense plaques in transmission electron microscopy. Merged endothelial cells initially form vessel tubes with incomplete basal laminae, whereas the maturation and stabilization of the newly formed endothelium are characterized by the complete basal lamina and the adhesion of pericytes at the capillary wall. Apart from sprouting activities, intussusceptive processes were found in our study for the vascular neoformation in biomaterial, which so far have not been described. The intussusceptive neoformation is commenced by the invagination of opposing capillary walls and the development of a bilayer followed by the sprouting of α-smooth muscle actin-positive pericytes [27] or fibroblasts. The accumulation of platelet factors in the biomaterial did not induce a significant up-regulation of vessel neoformation. In this respect, it is of interest that also in another study platelet-derived growth factors (PDGFs) did not stimulate endothelial cells directly, but influenced maturation of newly formed vessel tubes by activation of pericytes [27]. In

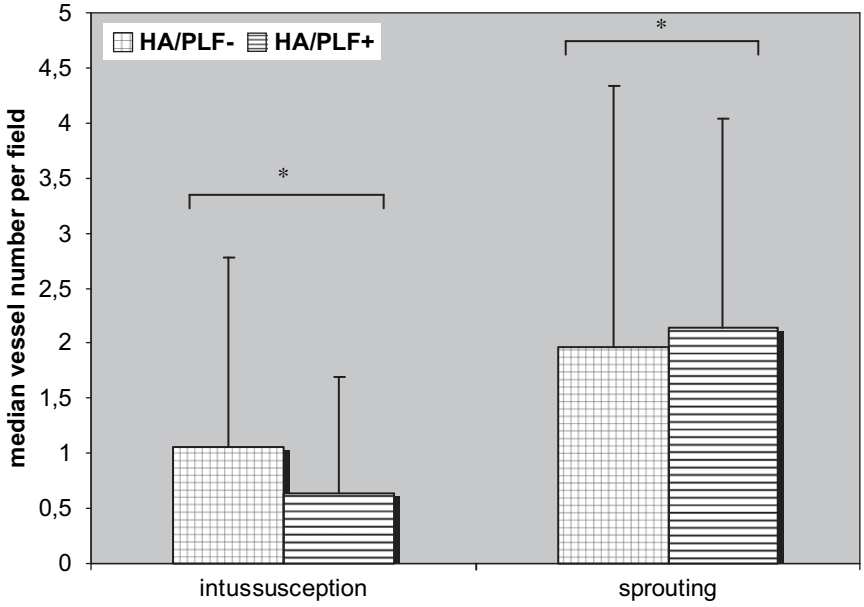

Fig. 6. Median number ± SD of vessel sprouting and intussusception per field in defects filled with HA/PLF− and HA/PLF+, day 20 after implantation, $^{*}p > 0.05$.

contrast, vascular endothelial growth factor (VEGF) plays a key role in the induction of angiogenesis. However, the VEGF-concentration of the autologous lysed platelets applied in our study remained below the detection limit of 10 pg/ml by ELISA. Nevertheless, the detected variants $VEGF^{189}$ and $VEGF^{205}$, identified by Western blot in this study, can be explained as a result of a hypoxia-induced increased TGF-β release from platelets leading to stimulation of VEGF expression in megakaryocytes [36]. Similarly, in a fracture model with rats Uchida et al. [37] also demonstrated $VEGF^{189}$ expression at day 5 post-operation. These authors, however, found

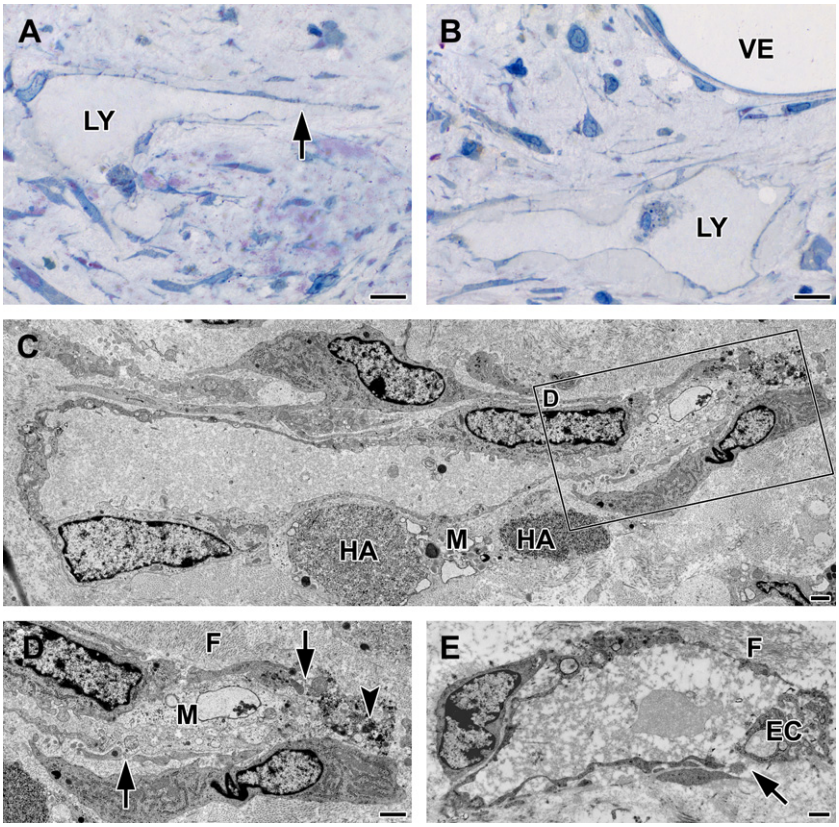

Fig. 7. Lymphangiogenesis. (A) Lymphatic vessel with open endothelium (black arrow) surrounding cells with incorporated hydroxyapatite material, (B) blind-ended sprouting lymphatic vessel, diameter approximately 40 μm, intravasal hydroxyapatite particle after degradation, semithin section with toluidine blue staining, and bar = 10 μm. HA/PLF−, day 20 after implantation. (C) Lymphatic vessel and macrophages. (D) Degenerated macrophage (arrowhead), degraded HA extracellular close to a lymphatic vessel (black arrows). (E) Anchoring filaments of endothelium and an open pore (black arrow) of a lymphatic vessel. Transmission electron microscopy, all bars = 1 μm, HA/PLF−, day 20 after implantation, LY = lymphatic vessel, VE = vein, HA = hydroxyapatite, M = macrophage, EC = endothelial cells, and F = anchoring filament.

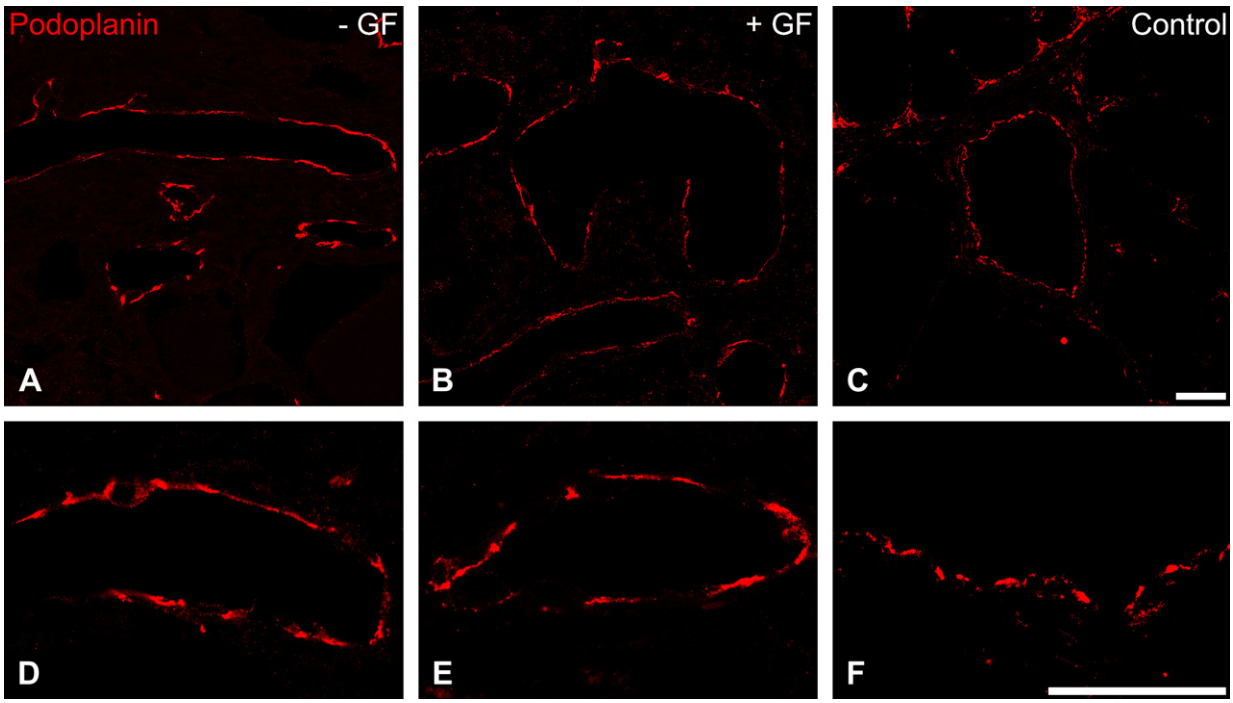

Fig. 8. Confocal fluorescence microscopy images of podoplanin-labelled lymphatic vessels in HA/PLF− implant (A, D) and HA/PLF+ implant (B, E), day 20 after implantation. For positive control, afferent vessels of a lymphatic node were labelled (C, F), all bars = 20 μm, and GF = growth factors.

a down-regulation of $VEGF^{189}$ protein after day 11 post-operation. Osteoblasts did not show any $VEGF^{189}$ immunoreactivity. In another investigation it could be demonstrated that $VEGF^{189}$ and $VEGF^{205}$ bind to remnants of heparansulfate, are less diffusible and possess less angiogenic potential than the small splice variants $VEGF^{121}$ and $VEGF^{165}$ [38,39]. This could explain the missing induction of the angiogenetic potential of the larger VEGF variants in our study.

Immunohistochemistry revealed VEGFR-2 positive cells in granulation tissue between hydroxyapatite particles. These cells showed the morphological structure of endothelial progenitor cells with a vesicular nucleus and incomplete endothelial sprouting in transmission electron microscopy [17].

It is known from the literature [17] that as soon as blood islands appear, VEGF is expressed, inducing cell differentiation, i.e. differentiation of pluripotent haematopoietic cells to angioblasts. The further differentiation to endothelial cells is regulated by the interaction of VEGF and its receptor VEGFR-2. These differentiation processes have been described so far in embryogenesis, cancer, inflammation and wound healing [17–20]. De novo lymphangiogenesis also occurs in these processes. The differentiated lymphatic vessel system maintains normal tissue pressure by draining the protein-rich lymph from an inflammatory tissue and removes phagocytose debris and inflammatory cells. Lymphatic endothelial cells can be distinguished from blood endothelial cells by the expression of specific markers, including lymphatic vessel endothelial receptor-1 (LYVE-1), prospero related homeobox gene-1 (Prox-1), podoplanin and VEGFR-3. Podoplanin co-expressed with VEGF-3 in lymphatic capillaries, and both antigens have been employed as a high-sensitive lymphoangiogenic marker in normal and pathological tissue samples [23,25,34,40,41].

In addition, Breitender-Geleff et al. [42] also demonstrated the specificity of podoplanin expression in lymphatic but not in blood vessels in angiosarcoma tissue.

In connective tissue between hydroxyapatite particles, we observed an abundant number of degenerated, hydroxyapatite-filled macrophages. Maruyuma et al. [41] have described that monocyte/macrophage express VEGFR-3 protein and contribute to the induction of de novo lymphangiogenesis in a corneal inflammation model. Because we found macrophages near vessel-like structures in our study a podoplanin antibody was applied to distinguish whether these vessels were of lymphatic origins or not.

As early as on day 10 after implantation, we were able to verify lymphatic vessels with typical structures in connective tissue between hydroxyapatite particles by using transmission electron microscopy, and positive podoplanin(+) immunolabelling.

At days 10 and 20 after operations we always found hydroxyapatite-filled macrophages close to these lymphatic vessels. In agreement with the studies of Jeltsch et al. [24] and Oh et al. [29], we observed that lymphatic capillaries consist of a thin-walled single layer of non-fenestrated endothelial cells and are not invested with mural cells.

In our study the endothelium of lymphatic capillaries exhibited typical morphological characteristics such as overlapping junctions between endothelial cells and large pores for the absorption of lymph as well as filaments which might allow the contraction of these capillaries leading to directed transport to the lymph. Furthermore, a basal lamina was missing, and the diameter of lymphatic vessels was usually considerably bigger than that of the blood vessels. The lymphatic network was characterized by open- or blind-ended vessels, which might drain extravasated fluids from the granulation tissue to the venous circulation [43].

According to Edwards et al. [25] lymphatic vessels could not be identified in cortical and cancellous bone. We presume that the occurrence of lymphatic vessels in the bone graft might be regarded as a temporary phenomenon. These results suggest that lymphatic vessels might play an essential role in fluid transport in hydroxyapatite degradation.

The highest degradation rate of the nanoparticulate hydroxyapatite Ostim® in metaphyseal bone defects, combined with the highest cellular resorptive activity of macrophages, was found within the first 6–8 weeks after implantation of the bone substitute material in a sheep model. After this time-period the number of

Ostim®-adhering macrophages decreased. Due to the osteoconductive reaction after 2 months defects were bridged and formed bone which also surrounded the nanoparticulate hydroxyapatite particles (E. Dingeldein, unpublished observations).

Possibly, the inflammatory reaction with increased activity of macrophages induces the degradation of the bone substitute material.

However, no quantitative differences in the number of podoplanin-labelled lymphatic vessels between HA/PLF− and HA/PLF+ groups were observed in our study. This indicates that neither platelet cytokines nor the increased number of macrophages induced by platelet factors enrichment of the hydroxyapatite implants – as observed in a previous study from our group [44] – influenced de novo lymphangiogenesis in the hydroxyapatite bone substitute material.

The results from this study suggest that the specific growth factor content in PLF bound to HA used does not seem to (a) influence the availability of vascular progenitor cells or (b) show any effects on new vessel formation.

The missing effect of PLF on the microvascularisation of the biomaterial might be related to the affinity of the compounds of the PLF to the hydroxyapatite with the formation of cytokine–HA complexes that do not bind to the membrane receptors of the target cells. Another explanation could be that those complexes are phagocytosed and, therefore, inactivated by the PLF induced increase of TRAP positive cells [44].

The ELISA testing of the platelet factor mixture revealed only very low levels of VEGF which is the most important pro-angiogenetic cytokine. Therefore, VEGF-induced stimulation of angiogenesis by PLF application to the biomaterial cannot be expected.

At the time of the implantation of the PLF-loaded biomaterial there may not be sufficient vascular progenitor cells with respective receptors to be present. The current work shows that a strong microvascularisation was achieved by the unloaded HA most likely due to its own high pro-angiogenetic potential that cannot be further increased by the additional application of PLF. These speculations need specification in following examinations.

5. Conclusions

In this study we describe the formation of blood vessels by sprouting and intussusceptive processes as well as angioblast differentiation in a nanoparticulate hydroxyapatite implant, independent of local application of platelet growth factors. In addition to blood vessel formation, the occurrence of lymphatic capillaries in the vicinity of the hydroxyapatite implant material was demonstrated by transmission electron microscopy and by immunofluorescence for podoplanin, a specific marker for lymphatic endothelial cells. Since degenerated macrophages, containing absorbed hydroxyapatite material, were found at the openings of these lymphatic vessels, we propose the macrophages in conjunction with the lymphatic system are involved in the biodegradation and removal of the synthetic hydroxyapatite bone substitute material.

Acknowledgment

This work was supported by the Federal Ministry for Education and Research (*B*undes*m*inisterium für *B*ildung und *F*orschung, BMBF; Tissue engineering, No: PTJ-BIO/0312741), Bonn, Germany.

References

[1] Williams SK, Kleinert LB, Hagen KM, Clapper DL. Covalent modification of porous implants using extracellular matrix proteins to accelerate neovascularization. J Biomed Mater Res A 2006;78:59–65.
[2] Sung HJ, Meredith C, Johnson C, Galis ZS. The effect of scaffold degradation rate on three-dimensional cell growth and angiogenesis. Biomaterials 2004; 25:5735–42.
[3] Kidd KR, Nagle RB, Williams SK. Angiogenesis and neovascularization associated with extracellular matrix-modified porous implants. J Biomed Mater Res 2002;59:366–77.
[4] Augustin HG. Tubes, branches, and pillars. The many way of forming a new vasculature. Circ Res 2001;89:645–7.
[5] Flamme I, Frolich T, Risau W. Molecular mechanism of vasculogenesis and embryonic angiogenesis. J Cell Physiol 1997;173:206–10.
[6] Beck L, D'Amore PA. Vascular development: cellular and molecular regulation. FASEB J 1997;11:365–73.
[7] Carmeliet P, Jain RK. Angiogenesis in cancer and other disease. Nature 2000; 407:249–57.
[8] Bussolino F, Mantovani A, Persico G. Molecular mechanism of blood vessel formation. Trends Biochem Sci 1997;22:251–6.
[9] Risau W. Mechanism of angiogenesis. Nature 1997;386:671–4.
[10] Djonov V, Baum O, Burri PH. Vascular remodeling by intussusceptive angiogenesis. Cell Tissue Res 2003;314:107–17.
[11] Hanahan D, Folkmann J. Patterns and emerging mechanisms of the angiogenic switch during tumorigenesis. Cell 1996;86:353–64.
[12] Ni H, Yuen PS, Papalia JM, Trevithick JE, Sakai T, Fässler R, et al. Plasma fibronectin promotes thrombus growth and stability in injured arterioles. Proc Natl Acad Sci U S A 2003;100:2415–9.
[13] Gerhardt H, Betsholtz C. Endothelial–pericyte interactions in angiogenesis. Cell Tissue Res 2003;314:15–23.
[14] Carmeliet P. Angiogenesis in health and disease. Nat Med 2003;9:653–60.
[15] Burri PH, Tarek MR. A novel mechanism of capillary growth in the rat pulmonary microcirculation. Anat Rec 1990;228:35–45.
[16] Zhou A, Egginton S, Hudlicka O, Brown MD. Internal division of capillaries in rat skeletal muscle in response to chronic vasodilator treatment with alpha1-antagonist prazosin. Cell Tissue Res 1998;293:293–303.
[17] Risau W, Flamme I. Vasculogenesis. Annu Rev Cell Dev Biol 1995;11:73–91.
[18] Patan S. Vasculogenesis and angiogenesis as mechanisms of vascular network formation, growth and remodeling. J Neurooncol 2000;50:1–15.
[19] Crosby JR, Kaminski WE, Schatteman G, Martin PJ, Raines EW, Seifert RA, et al. Endothelial cells of hematopoietic origins make a significant contribution to adult blood vessel formation. Circ Res 2000;87:728–30.
[20] Asahara T, Murohara T, Sullivan A, Silver M, Van der Zee R, Li T, et al. Isolation of putative progenitor endothelial cells for angiogenesis. Science 1997;275: 964–7.
[21] Ramirez MI, Pollack L, Milien G, Cao YX, Hinds A, Williams MC. The alpha-isoform of caveolin-1 is a marker of vasculogenesis in early lung development. J Histochem Cytochem 2002;50:33–42.
[22] Oliver G, Detmar M. The rediscovery of the lymphatic system: old and new insights into the development and biological function of the lymphatic vasculature. Genes Dev 2002;16:773–83.
[23] Parsons-Wingerter P, McKay TL, Leontiev D, Vickerman MB, Condrich TK, Dicorleto PE. Lymphangiogenesis by blind-ended vessel sprouting is concurrent with hemangiogenesis by vascular splitting. Anat Rec A 2006;288: 233–47.
[24] Jeltsch M, Tammela T, Alitalo K, Wilting J. Genesis and pathogenesis of lymphatic vessels. Cell Tissue Res 2003;314:69–84.
[25] Edwards JR, Williams K, Kindblom LG, Meis-Kindblom JM, Hogendoom PC, Hughes D, et al. Lymphatics and bone. Hum Pathol 2008;39:49–55.
[26] Auguste P, Javerzat S, Bikfalvi A. Regulation of vascular development by fibroblast growth factors. Cell Tissue Res 2003;314:157–66.
[27] Betsholtz C, Karlsson L, Lindahl P. Developmental roles of platelet-derived growth factors. Bioessays 2001;23:494–507.
[28] Esser S, Wolburg K, Wolburg H, Breier G, Kurzchalia T, Risau W. Vascular endothelial growth factor induces endothelial fenestrations in vitro. J Cell Biol 1998;23:947–59.
[29] Oh SJ, Jeltsch MM, Birkenhager R, McCarthy JE, Weich HA, Christ B, et al. VEGF and VEGF-C: specific induction of angiogenesis and lymphangiogenesis in the differentiated avian chorioallantoic membrane. Dev Biol 1997;188:96–109.
[30] Tadic D, Epple M. A thorough physicochemical characterisation of 14 calcium phosphate-based bone substitution materials in comparison to natural bone. Biomaterials 2004;25:987–94.
[31] Tadic D, Peters F, Epple M. Continuous synthesis of amorphous carbonated apatites. Biomaterials 2002;23:2553–9.
[32] Welter H, Wollenhaupt K, Tiemann U, Einspanier R. Regulation of the VEGF-system in the endometrium during steroid-replacement and early pregnancy of pigs. Exp Clin Endocrinol Diabetes 2003;111:33–40.
[33] Donath K, Breuner GA. Method for the study of undecalcified bones and teeth with attached soft tissue. J Oral Pathol 1982;4:316–26.
[34] Cimpean AM, Raica M, Ivzenariu DA, Tatucu D. Lymphatic vessels identified with podoplanin. Comparison of immunostaining with free different detection systems. Rom J Morphol Embryol 2007;48:139–43.
[35] Laschke MW, Witt K, Pohlemann T, Menger MD. Injectable nanocrystalline hydroxyapatite paste for bone substitution: in vivo analysis of biocompatibility and vascularization. J Biomed Mater Res B 2007;82:494–505.
[36] Steinbrech DS, Mehrara BJ, Saadeh PB, Greenwald JA, Spector JA, Gittes GK, et al. VEGF expression in an osteoblast-like cell line is regulated by a hypoxia response mechanism. Am J Physiol Cell Physiol 2000;278:853–60.
[37] Uchida S, Sakai A, Kudo H, Otomo H, Watanuki M, Tanaka M, et al. Vascular endothelial growth factor is expressed along with its receptors during the

healing process of bone and bone marrow after drill-hole injury in rats. Bone 2003;32:491–501.
[38] Vincenti V, Cassano C, Rocchi M, Persico G. Assignment of the vascular endothelial growth factor gene to human chromosome 6p21.3. Circulation 1996; 15:1493–5.
[39] Gerber HP, Vu TH, Ryan AM, Kowalski J, Werb Z, Ferrara N. VEGF couples hypertrophic cartilage remodeling, ossification, and angiogenesis during enchondral bone formation. Nat Med 1999;5:623–8.
[40] Al-Rawi MA, Mansel RE, Jiang WG. Molecular and cellular mechanisms of lymphangiogenesis. Eur J Surg Oncol 2005;31:117–21.
[41] Maruyuma K, Asai J, Li M, Thorne T, Losordo DW, D'Amore PA. Decreased macrophage number and activation lead to reduced lymphatic vessel formation and contribute to impaired diabetic wound healing. Am J Pathol 2007;170:1178–91.
[42] Breitender-Geleff S, Soleiman A, Kowalski H, Horvat R, Amman G, Kriehuber E, et al. Angiosarcomas express mixed endothelial phenotypes of blood and lymphatic capillaries: podoplanin as a specific marker for lymphatic endothelium. Am J Pathol 1999;154:386–94.
[43] Adams RH, Alitalo K. Molecular regulation of angiogenesis and lymphangiogenesis. Nat Rev Mol Cell Biol 2007;8:464–78.
[44] Kilian O, Wenisch S, Alt V, Lauer M, Fuhrmann R, Dingeldein E, et al. Effects of platelet factors on biodegradation and osteogenesis in metaphyseal defects filled with nanoparticular hydroxyapatite – an experimental study in minipigs. Growth Factors 2007;25:191–201.